HHS Public Access

Author manuscript

Small. Author manuscript; available in PMC 2023 June 01.

Published in final edited form as:

Small. 2022 June ; 18(25): e2201561. doi:10.1002/smll.202201561.

Designing A Mucoadhesive ChemoPatch to Ablate Oral Dysplasia for Cancer Prevention

Xiaoqin Liu[1],

Qian Li[2],

Yang Wang[3],

Madeleine Crawford[1],

Parnit K. Bhupal[1],

Xiuqing Gao[3],

Huan Xie[3],

Dong Liang[3],

Yi-Shing Lisa Cheng[4],

Xiaohua Liu[2],

Robert Y.L. Tsai[1,5,*]

[1]Institute of Biosciences and Technology, Texas A&M Health Science Center; Houston, TX 77030, USA

[2]Department of Biomedical Sciences, Texas A&M University College of Dentistry; Dallas, TX 75246, USA

[3]College of Pharmaceutical Sciences, Texas Southern University; Houston, TX 77004, USA

[4]Department of Diagnostic Sciences, Texas A&M University College of Dentistry; Dallas, TX 75246, USA

[5]Department of Translational Medical Sciences, Texas A&M Health Science Center; Houston, TX 77030, USA

Abstract

Oral cancer (OC) has a high mortality rate, and its treatment often causes debilitating complications. More than 90% of oral cancers are oral squamous cell carcinomas (OSCCs) that may develop from clinically recognizable oral premalignant lesions (OPLs). To eradicate OPLs before they turn into cancers, we develop a non-invasive topical formulation based on a novel combination of synergistically acting oxaliplatin (OXP) and mycophenolate (MPS) embedded in a controlled-release mucoadhesive patch fabricated by computer-aided 3-dimentional printing. After multiple rounds of testing and optimization, a v6.4 chemopatch is designed, which shows sustained release of OXP and MPS *in vitro*, minimal side leakage of drugs, an average elastic modulus of 2.38 MPa, and suitable drug stability at 4°C or below for up to 12 months. *In*

*To whom correspondence should be addressed to: Robert Y.L. Tsai, 2121 W. Holcombe Blvd, Houston, TX 77030, robtsai@tamu.edu, (Tel): 1-713-677-7690; (Fax) 1-713-677-7512.

Conflict of Interest: The authors declare no potential conflict of interest

vivo analyses show that almost all patches adhere to the dorsal tongue surface for 4 hours, and display a sustained release of OXP and MPS to tongue tissue for 3–4 hours. When applied in the 4NQO-induced OPL rat model, the OXP-MPS patch significantly ablates dysplastic lesions with no damage to normal epithelial cells and minimal systemic absorption and side effects. This study reports the design of a novel mucoadhesive chemopatch as a noninvasive therapy to treat OPLs.

Graphical Abstract

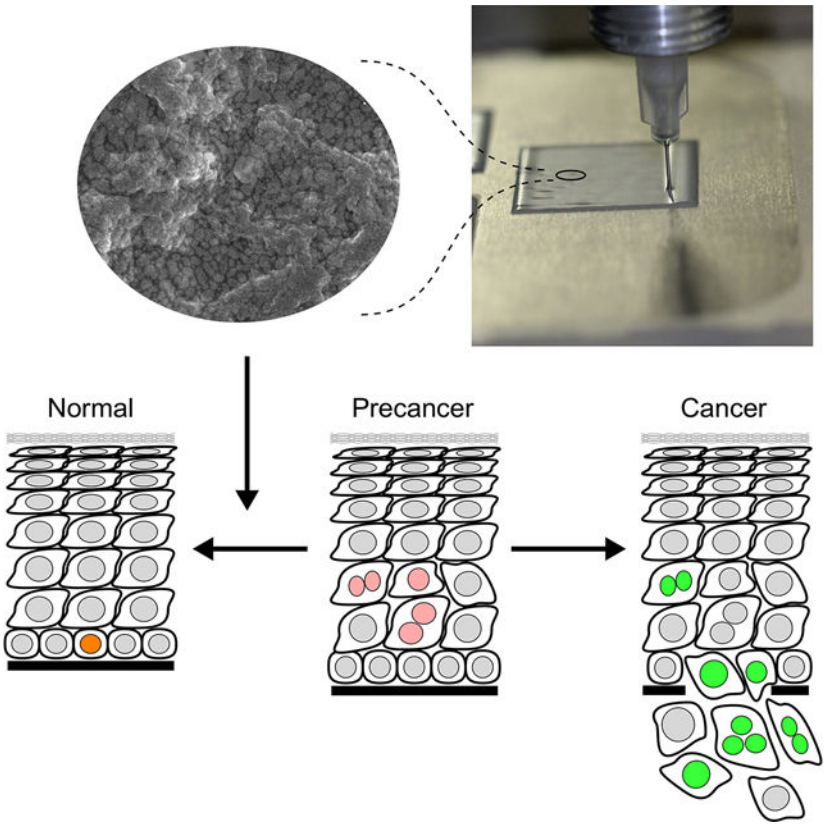

A novel mucoadhesive ChemoPatch is invented to provide a non-invasive therapeutic option for treating oral premalignant lesions, thereby preventing oral cancer formation. The design is based on a synergistically acting drug pairs, delivered by a 3-D-printed multi-layered mucoadhesive patch formulation in a controlled and sustained manner. Analyses of the mechanical, pharmacological, and biological properties of the ChemoPatch confirm its preclinical potential in treating oral precancer.

Keywords

3-D printing; topical drug delivery; bioengineering; biomaterial; mucoadhesive patch; oral premalignant lesion; oral cancer

1. Introduction

Oral cancer (OC) is the 8th most common cancer in males and 15th in females in the US, and its five-year survival rate (66%) is one of the lowest among all major cancer types [1, 2]. Patients who survive OC often have to live with impaired functions and disfiguration caused by the treatment. More than 90% of OCs are oral squamous cell carcinomas (OSCCs) that may develop from clinically visible leukoplakia or erythroplakia. Leukoplakia is wide spread, affecting 1.5–4.3% of the world population [3]. The malignant transformation rates of oral premalignant lesions (OPLs) correlate with the grade of oral epithelial dysplasias (OED), occurring at 4–11% for low-grade OEDs and 20–43% for high-grade OEDs [3]. While some low-grade OEDs may spontaneously regress, high-grade OEDs typically persist. Given its high mortality rate and treatment-related complications, the most cost-efficient way to manage OCs is to eradicate OEDs before they become cancers. Current therapeutic options for OEDs include surgical resection, laser ablation, cryotherapy, and systemic medications. Their recurrence rates remain substantial (9–35% for surgical or laser treatment; 47–56% for non-surgical intervention) [4–10]. Surgical excision and laser ablation of large-sized lesions also cause severe discomfort and scar formation and require specialized clinics [11]. Systemic medication provides field treatment but is limited by systemic side effects and high recurrence. There is a critical unmet need for an effective non-invasive treatment for low-grade OEDs.

IMP dehydrogenase (IMPDH) inhibitors have reemerged as a potential anti-cancer agent in the last few years [12]. Mycophenolic acid (MPA) is a noncompetitive and reversible inhibitor of both IMPDH1 and IMPDH2 and has been used for many years as an immunosuppressant for organ transplantation and psoriasis [13]. In early clinical trials, the anti-cancer potential of MPA was diminished largely by the conversion of most circulating MPA (> 95%) into an inactive glucuronide derivative in the liver [14] and its dose-limiting gastrointestinal toxicity [15]. We have previously reported a strong synergistic activity of MPA to potentiate the cytotoxic effect of oxaliplatin (OXP) in oral squamous cell carcinoma (OSCC-25) cells [16], which is in line with an observed correlation between the use of MPA and a decreased incidence in skin cancer and lymphoproliferative disorders in patients with kidney transplants [17, 18].

Oral drug delivery design has progressed rapidly with the advancement in polymer technologies [19]. Compared to systemic administration, topical application of OXP and MPA offers the advantages of achieving higher tissue-to-plasma drug concentrations, escaping the hepatic first-pass metabolism, and minimizing systemic toxicities [20, 21]. Many topical delivery formulations are designed for systemic delivery and often dissolve instantaneously in the oral cavity. For local therapy, the main challenge is to withhold the delivery system on the mucosal surface for sufficient time to allow sustained and controlled release of drugs on lesion-specific sites [22].

To achieve these objectives, we used a computer-aided design (CAD) three-dimensional (3-D) printing technique to formulate a novel mucoadhesive patch for topical delivery of OXP and MPA as a noninvasive OED therapy. Compared to the conventional solution casting/molding method, the 3-D printing technology provides the advantages of fabricating

the patch with a well-defined multilayer structure and controlling the drug formulation in each layer with high precision, thereby allowing us to achieve: (1) a unidirectional release of drugs from the patch to the oral mucosa to minimize damage to the surrounding healthy oral tissue; (2) controlled and synchronized release of multiple drugs (*i.e.*, OXP and MPS), and (3) batch-to-batch consistency in the thickness of layers and the evenness of OXP and MPS distribution within the patch, which is critical for future GMP manufacturing and clinical application. The final v6.4 patch design was tested for its *in vitro* and *in vivo* properties, as well as *in vivo* toxicity and efficacy in healthy and 4NQO-induced oral carcinogenesis rat models. 4NQO is a synthetic water-soluble carcinogen that introduces oxidative stress and G-to-A mutations, closely resembling genomic insults caused by tobacco-related carcinogens [23, 24]. Rodents treated with 4NQO develop oral carcinogenic lesions ranging from hyperplasia to OED and OSCC that bear high histological and molecular resemblance to human diseases [25]. Here, we report the engineering and testing of a novel mucoadhesive chemopatch as a new non-invasive OED therapy *in vitro* and in a preclinical model.

2. Results

2.1 MPA synergizes the cytotoxicity of OXP in dysplastic oral keratinocyte (DOK) cells

We previously discovered a strong cytotoxic synergy between MPA and paclitaxel (combination index [CI] = 0.12) or OXP (CI = 0.25) in OSCC-25 cells [26]. Here, we determined the chemo-synergizing effect of MPA in combination with 5-FU, paclitaxel, or OXP in DOK cells. The IC_{50} concentrations of MPA (13.30μM), OXP (1.67μM), 5-FU (3.33μg/mL), and paclitaxel (0.41nM) in DOK cells were determined by their dose response curves based on the MTT assay. The interaction between MPA and 5-FU, paclitaxel, or OXP was analyzed by an Isoborogram. Synergistic (strong, moderate, and mild) and additive drug interaction were defined by their CI value range of 0.1–0.3, 0.3–0.7, 0.7–0.85, and 0.85–1.0, respectively. Five different ratios of mixture (4:1, 2:1, 1:1, 1:2, and 1:4) were tested for each drug combination, with the 1:1 ratio representing each drug at equal amounts with respect to their IC_{50} concentrations. In DOK cells, MPA showed strong cytotoxic synergy with OXP at all five ratios tested but only mild-to-moderate synergy with 5-FU (CI = 0.56) or paclitaxel (CI = 0.81) (Figure 1A). Based on the synergy data, a mucoadhesive patch was designed to topically deliver a two-drug combination of OXP and MPA.

2.2 Formulation and optimization of the OXP-mycophenolate (MPS) patch

A CAD-3D printing platform was used to fabricate the mucoadhesive chemopatch (Figure 1B). The principal design of the patch consisted of a drug-embedded mucoadhesive layer on a supportive frame (Tegaderm™), which served as a waterproof barrier to ensure unidirectional drug release. The mucoadhesive drug layer was a mixture of OXP, MPS, and three bioadhesive materials. MPS was used for its higher water solubility compared to MPA. Different amounts and component subtypes of the three bioadhesive materials were tested to identify a formulation with the best mucoadhesive properties. The targeted amounts of OXP and MPS to be delivered to the oral mucosa were estimated by the following calculations. The IC_{50} concentrations of OXP and MPS for DOK cells are 1.67μM (= 0.66μg/mL) and 13.30μM (= 4.55μg/mL), respectively. The volume of a circular lesion with a size of 8mm in diameter and 2mm in depth is 0.1mL [$0.2\times(0.4)^2\times\pi = 0.1cm^3$].

To reach their IC_{50} concentrations for DOK cells in this hypothetical lesion, 0.066μg of OXP and 0.455μg of MPS should be delivered. Assuming that the half-life of OXP and MPS in the mucosa is 30 minutes (50% turnover in 30 minutes), 0.33μg of OXP (= 0.066 + 8×0.066÷2) and 2.275μg of MPS (= 0.455 + 8×0.455÷2) (1:6.9 in weight) should be delivered over a 4-hour therapeutic window, assuming a sustained release profile, to achieve average tissue concentrations of 1× IC_{50} concentrations of OXP and MPS individually or 2× IC_{50} concentration of the OXP-MPS combination (½ OXP + ½ MPS).

A major challenge in formulating a two-drug delivery device is to accommodate or, better, to synchronize their release profiles, which depends on their respective solubility and stability in the bioadhesive matrix. We began by embedding 3mg of OXP and 20mg of MPS into a single-layered square sheet (30mm×30mm×20μm) and measured the *in vitro* drug release profiles in water over a 4-hour time window. Multiple revisions on the formulation design were made to improve the drug release profiles (Figure S1), leading to the design of a two-layered OXP-MPS patch (v6) in 20μm thickness (Figure 1C1). Scanning electron microscopy (SEM) showed that the surface of the patch exhibited a granular structure, which might help facilitate its adhesion to the mucosal tissues (Figure 1C2). Five variations of the v6 chemopatch were tested, each containing two bioadhesive drug layers with the same total amount of MPS (14.13μg in a 5mm-diameter circular disc) and different amounts of OXP. The v6.1 to v6.5 patch contained a total amount of 7.06μg, 3.5μg, 1.77μg, 1.06μg, and 7.06μg OXP (for a 5mm-diameter disc) distributed in a 1:2 ratio between the top and bottom layers, adjusted to pH 6.0 for the v6.1–6.4 patches and pH 7.4 for the v6.5 patch. The cumulative release profiles of OXP and MPS at 10 minutes (m), 30m, 1 hour (h), 2h, 3h, and 4h were quantified by UPLC-PDA (Ultra-Performance Liquid Chromatography with Photo-Diode-Array detector) and calculated as percentages of their respective total extractable amounts. Within 10m, 30–35% of OXP was released from the v6.1-v6.4 patches and 13% was released from the v6.5 patch. All five patches showed a steady release profile after 30m and reached 68–93% at 4h, with the v6.4 patch showing the highest release efficiency (Figure 1D1). MPS showed a zero-order kinetic release profile from 0–4h and a 50% release efficiency at the end of 4h (Figure 1D2). Of the five different patch variations, only the v6.4 patch could reach close to the targeted 6.9:1 ratio (dashed line) of the cumulative released MPS:OXP amounts by weight over a 4h period (Figure 1E). The amounts of OXP and MPS released from a 5mm-diameter circular v6.4 patch were 855ng and 5252ng, respectively, about 6 times higher than the estimated amounts required to reach their respective IC_{50} concentrations in the tissue (128.9ng and 888.7ng). We also created a higher-dose patch (1.5×) and found that the v6.4 patch and the 1.5× patch performed equally (Figure S2). Based on these findings, the v6.4 patch design was used for the following testing.

2.3 In vitro properties of the OXP-MPS v6.4 patch

Drug leakage from the side of the v6.4 patch was measured in a Franz Diffusion Cell apparatus and calculated as a percentage of the total amount embedded in the patch. Only a trace amount of MPS (3.7% ± 0.61%, SEM) leaked from the side of the patch during a 4h period and no OXP was detected (Figure 2A). *Ex vivo* mucosal permeation of OXP and MPS was measured on a piece of porcine mucosa (5–7mm thickness). At the end of 4h, 45.1% (± 7.7%) of the MPS was released and retained in the mucosa, and only a very

small fraction (0.5%) of the MPS passed through the mucosal/submucosal tissue to reach the receptor chamber (Figure 2B). No OXP was detected in the receptor chamber or in the *ex vivo* mucosa throughout the 4h duration. It has been reported that OXP undergoes rapid conversion to Pt(dach)Cl(OH) (monochloro DACH platin) and Pt(dach)Cl_2 (dichloro DACH platin) in the presence of chloride ion. These chloride derivatives of OXP are not detectable by current available assays. In support, we found that OXP is converted by chloride in a time and concentration-dependent manner but remains stable in NaPi, glucose, or H_2O solutions, as well as in solutions containing the bioadhesive material components (Figure S3). It is worth noting that even though these chloride derivatives of OXP are not detectable, they are known to be as cytotoxic as OXP in cellular assays [27–29].

The average elastic modulus of five independent v6.4 patches was determined to be 2.38 MPa (± 0.63 SD) using a TestResources System (Figure 2C, Figure S4). The elasticity of the v6.4 patch was shown by the stress-strain curves that it could be stretched for over 30% longer than its original length without breaking (arrows). Adhesion force is widely used to characterize the bioadhesive strength of a mucoadhesive patch. It is defined by the force required to detach the patch from the mucosal surface that it contacts. The average adhesion force of the OXP-MPS v6.4 patch mounted on porcine buccal mucosa was 1.29 ± 0.30 N (mean ± s.d.) (Figure S5). This finding indicates that the patch can be readily peeled off after drug release. To determine drug stability in the patch, v6.4 patches were formulated and stored at different temperatures (25°C, 4°C, or −20°C) for 1 day (1d), 4d, 7d, 14d, 21d, 28d, 2, 4, 6, 9, and 12 months. OXP and MPS remaining in stored patches were extracted, quantified by UPLC-PDA, and compared to the amounts extracted from freshly formulated patches (0d). Our results demonstrated that OXP in the v6.4 patch remains stable for at least 12 months if stored at 4°C or −20°C, but becomes rapidly degraded in 4d when kept at 25°C (Figure 2D1). MPS remains stable for 6m even at 25°C. If stored at −20°C and 4°C, MPS is stable for 12 months (Figure 2D2).

2.4 Ex vivo and in vivo mucoadhesiveness

Ex vivo mucoadhesiveness of the OXP-MPS v6.4 patch was tested on a piece of porcine buccal mucosa completely submerged in simulated saliva. About 50% of the patches stayed on the mucosa after 2h and >80% of the patches detached from the mucosa after 3.5h (Figure 3A). The average residence time was 2.4h. The *in vivo* mucoadhesiveness of the OXP-MPS v6.4 patch on oral mucosal surface was determined at different sites. Circular patch discs (4mm or 3mm diameter) were placed on the anterior dorsal tongue, posterior dorsal tongue, and buccal mucosa (Figure 3B1). Patch retention was examined at fixed timepoints while animals were kept under anesthesia. Our results showed that almost all patches stay on the mucosa for at least 4h, regardless of the patch size or the placement site (Figure 3B2).

2.5 In vivo drug release profiles

The release profiles of OXP and MPS from the v6.4 patch to rat oral mucosa and blood were measured by placing a 4mm-diameter circular patch on the dorsal tongue surface for 0.5h, 1h, 2h, 3h, or 4h. At the end of each timepoint, tongue tissue and plasma samples were collected. In two additional groups, patches were applied for 4h and samples were

collected at 8h or 12h after the initial patch placement. Our results showed that the amount of MPS released into the tongue tissue reached 3μg (40% of the embedded amount) in 0.5h, remained relatively constant for the first 4h, and decreased rapidly to < 5% at the 8h timepoint (4h after patch removal) (Figure 4A). The amount of OXP accumulated in the tongue tissue was about 65ng (21% of the embedded amount) in 0.5h, decreased to 30ng in 2h and 10.6ng in 4h, and became undetectable in after 8h (Figure 4B). The plasma concentration of MPS with a 4h patch application was very low, limited to a peak concentration of 6.5ng/mL in 8h (Figure 4C). OXP was undetectable. These results demonstrated that the v6.4 patch provides a steady release of MPS in oral mucosa for 4h and OXP for 0.5h. The drop of OXP from 30m to 4h is consistent with its rapid metabolism by the tissue chloride ion. Although undetectable by current Liquid Chromatography with tandem Mass Spectrometry (LC-MS/MS) methods, these chloride metabolites of OXP may still be bioactive [27–29].

2.6 Efficacy of the OXP-MPS v6.4 patch in treating OEDs in a 4NQO rat model

The efficacy of the OXP-MPS v6.4 patch in treating OEDs *in vivo* was tested using a 4NQO Sprague Dawley (SD) rat model (Figure S6A). Animals with pathologically confirmed low-grade OEDs were randomly divided to receive the OXP-MPS (O-M) chemopatch or non-medicated blank patch, collected for histological evaluation after a 5d treatment course and a 10d recovery period (Figures S6B and S6C). Our data demonstrated that 88.9% of low-grade OEDs treated with the OXP-MPS patch showed a complete reversion to normal epithelium with normal cellular maturation, whereas only 20% of those treated with the blank patch reverted to normal epithelium (Figure 5A1, 5B1, 5C). Only 11.1% of low-grade OEDs treated with the OXP-MPS patch remained as dysplastic and 80% of those treated with the blank patch either remained as low-grade OEDs or advanced to invasive OSCC (Figure 5A2, 5B2, 5C). Chi-square analysis confirmed that the effect of the OXP-MPS patch in treating low-grade OEDs was significantly better than that of the blank patch ($p = 0.0027$) (Figure 5D). The plasma drug concentrations, sampled right before the placement of the last (5^{th}) patch, were not detectible for OXP and 4.52 (± 2.23) ng/mL for MPS in the OXP-MPS patch treated group. Ki67 staining showed that the numbers of mitotic cells in the basal and parabasal epithelium were indistinguishable between the blank and OXP-MPS patch groups before the treatment (Figure 5E1, orange bars). After the treatment, the numbers of mitotic cells decreased in both groups (Figure 5E1, blue bars). By comparison, the OXP-MPS patch-treated samples showed more decrease in their mitotic activity than did the blank patch-treated samples (Figure 5E2). These results demonstrate the efficacy of the OXP-MPS v6.4 patch in ablating low-grade OEDs *in vivo* and reducing the epithelial hyperactive proliferation.

2.7 Local and systemic toxicities of the OXP-MPS v6.4 patch in rats

Local and systemic toxicities associated with the v6.4 patch treatment were assessed by placing a 4mm-diameter patch on the dorsal tongue surface of healthy SD rats for 4h a day for 5 consecutive days and collecting tissues (tongue, kidney, liver, and intestine) for histological analysis and blood samples for liver function tests and complete blood count (CBC) two days after the last patch placement. H&E staining showed that the OXP-MPS patch did not damage the local oral epithelial morphology compared to the blank patch

(Figure 6A1). Immunostaining of Ki67 for proliferative cells and cleaved caspase 3 (CC3) for apoptotic cells showed that the OXP-MPS patch treatment did not affect the normal proliferative activity of basal cells, nor did it increase the number of apoptotic cells after 2 days of recovery (Figure 6A2–4). Two tailed t-tests confirmed that there was no difference in the levels of liver enzymes (ALP, ALT, and AST) (Figure 6B) or the numbers of RBCs and platelets in the peripheral blood between rats treated with the OXP-MPS vs. blank patch (Figure 6C). A mild decrease in WBCs was noted in the OXP-MPS-treated group compared to the blank-treated group (Figure 6C). No difference in histopathology (H&E), cell proliferation (Ki67), and cell death (CC3) was found in the intestine, kidney, or liver between rats treated with the OXP-MPS patch or the blank patch (Figure 6D and Figure S7). These results demonstrate that the OXP-MPS patch does not cause any discernible local or systemic toxicity except for mild leukopenia.

3. Discussion

While the majority of low-grade OEDs remain static for many years, a significant minority (4–11%) of them do develop into OSCC within a short period time (2–3 years). As there is no tool that can reliably predict the risk of low-grade OEDs in becoming cancer [30], management of those lesions often present a difficult decision to clinicians who must weigh their relatively low transformation rate against the definitive treatment complications, especially for those that are diffuse, multifocal, or recurrent. To meet the need for a non-invasive OPL therapy that is effective and easy to apply, we have designed a novel product based on a synergistically acting drug pair and a topically applied, controlled-release device to chemoablate OEDs. We determined its mechanical properties, mucoadhesiveness, and drug release profiles *in vitro* and *in vivo*, and demonstrated its efficacy in treating OEDs in a preclinical 4NQO rat model with no or minimal local/systemic toxicity.

3.1 Challenges in formulating a two-drug delivery device

Topical formulations have become increasingly important in clinical practices for intraoral diseases [19]. Novel adhesive polymers and multi-layer patch designs open up feasibility channels to allow sustained, site-specific, and unidirectional drug delivery [31]. The release of MPS from the v6.4 patch follows a zero-order kinetics *in vitro*. On the rat tongue mucosa, the v6.4 patch allows the sustained delivery of MPS to the tissue from 0.5h to 4h with an efficiency of 40–50% of the embedded amount. In the patch, MPS remains relatively stable for up to 12 months at or below room temperature. In contrast, the patch formulation of OXP was more challenging. In a uniform patch, the bulk of OXP (~90%) is released rapidly within 40–60m. To achieve a more sustained release profile, a 2-layer design was created to prolong the OXP release up to 3–4h (Figure 1D1). However, the cumulative amount of OXP in the mucosal tissue released from the patch appears to be lower compared to MPS, measuring at 21%, 9%, 8% 5%, and 3% of the embedded OXP amount after 0.5h, 1h, 2h, 3h, and 4h, respectively. The tissue release efficiency of OXP is 40% of the embedded amount. The drop in the tissue OXP amount over time is likely caused by the rapid biotransformation of OXP into chloride metabolites, *e.g.*, Pt(dach)Cl(OH), Pt(dach)Cl_2, and dihydrated oxaliplatin complex (DOC) [27]. Pt(dach)Cl_2 is transiently formed and accounts for only 2–8% of biotransformed OXP. DOC is “semi-stable” with a constantly opening and

closing oxalato ring. All three compounds are not commercially available and hence not measurable by currently available LC-MS/MS methods. Chloride biotransformation is not expected to diminish the therapeutic efficacy of OXP, as those metabolites were shown to be more cytotoxic than OXP in cellular assays [27–29]. The stability of OXP in the patch can be maintained for up to 12 months by keeping it at 4°C or −20°C but not at 25°C. Given that OXP is stable in the solid state, this instability of OXP in the patch after long-term storage at room temperature may be caused by adduct formation with trace amounts of solutes and solvents left in the patch formulation. When moving the patch product to clinical trials, this issue can be addressed by storing the chemopatch in the refrigerator or freezer before application, as well as a better product quality control to reduce residual chemicals during the dosage formulation process, to meet the FDA requirement of a minimum of 12-month storage stability.

3.2 Efficacy in treating 4NQO-induced OPLs in rats

Using a 4NQO-induced oral carcinogenesis rat model, we demonstrate that the OXP-MPS patch is very effective in eliminating dysplastic cells in low-grade OEDs. It can also reduce the hyperproliferative activity in the epithelium caused by 4NQO treatment. As three of the blank-treated OEDs later turned into OSCC, this result provides important proof-of-principle evidence to support the concept that chemoablation of OEDs by the v6.4 patch may prevent the future development of OSCC. The two cases showing lesion reversal in response to the blank patch treatment may be explained by the natural course of OPLs, complete removal of lesions during the biopsy, or lesion clearance by the post-biopsy healing process. Here, we use 4NQO-treated rats to model oral carcinogenesis in humans. The 4NQO rodent model displays several features characteristic of human OED and OSCC, including their lesion location, histology, gene expression profile, and formation of DNA adducts, which play a central role in the pathogenesis of tobacco-associated carcinogenesis [23, 32–35].

3.3 Safety profile

The systemic toxicity of locally applied OXP-MPS patches was evaluated based primarily on the reported side effects of OXP (leukopenia, thrombocytopenia, anemia, and liver, gastrointestinal and kidney dysfunctions) and MPS (leukopenia and gastrointestinal symptoms). OXP-induced peripheral sensory neuropathy is not tested. The only observed side effect of the OXP-MPS patch was a mild decrease in WBC count (4,500/μL). This effect is most likely caused by MPS and not OXP, which causes pancytopenia. Once entering the blood stream, the majority of OXP is rapidly transformed into sulfur-platinum complexes, which are biologically inactive [27, 36, 37], or reacts with serum G-globulins, albumin, and hemoglobin to forming non-cytotoxic complexes [38]. The local effect of the OXP-MPS patch on normal mucosal epithelium was determined by histology, cell proliferation, and cell death, which show no difference from the blank patch. These results establish that the OXP-MPS patch is relatively safe to use.

3.4 Clinical application and potential issues

Current OPL treatments have limitations due to their local or systemic side effects. Considering the risk-benefit ratio, using the more aggressive approach to remove low-grade OEDs is justified only if their risk of becoming OSCCs can be reliably and sensitively

predicted. However, such predictive markers are not yet available. Our drug-based device is designed to meet the need for a non-invasive method for treating low-grade OEDs that are difficult to manage by current therapeutic modalities, such as those that are large in size, diffuse, multifocal, and/or recurrent. Its efficacy and safety were determined in a preclinical model. Several issues remain to be addressed on the road toward its clinical implementation. Conceptually, it is not clear whether the OXP-MPS patch is able to eradicate transformed epithelial cells that are mitotically dormant, which may become a source of recurrence. In addition, human OEDs are molecularly and etiologically heterogeneous. We speculate that the v6.4 patch is likely to be effective in treating OEDs regardless of their etiologies, but a definitive proof will require future clinical trials. Given the heterogeneity of human lesions, it is also conceivable that not all lesions will be equally responsive to this treatment. It may be useful to develop marker-based strategies to identify treatment-sensitive lesions. The clinical applicability of the chemopatch therapy also depends on the accessibility to the sites of OEDs. In working with the preclinical model, which is considerably smaller in size compared to human lesions, we chose only lesions on the dorsal tongue surface for easy applicability and characterization.

4. Conclusion

We have developed a new mucoadhesive drug delivery device that combines the novelties of a synergistically acting drug combination to increase the efficacy and a patch formulation based on a 3-D-printed multi-layered design to provide sustained and controlled drug release at the lesion site to avoid hepatic first-pass metabolism and systemic toxicity. This chemopatch demonstrates the ability to ablate OEDs with minimal side effects in a preclinical model. It may hold the potential of changing the future landscape of low-grade OED treatment from an invasive surgical procedure to a non-invasive procedure that can be administered by a wider network of healthcare providers with better patient compliance. Finally, the design of a biocompatible and biodegradable mucoadhesive patch may also be used as a drug delivery platform with a tunable pharmacokinetic profile for a broad range of mucosal and dermal applications.

5. Experimental Section/Methods

5.1 Animal care and treatment

Animals were housed by the Program for Animal Resources at the TAMHSC-Houston campus and handled in accordance with the principles described by the Guide for the Care and Use of Laboratory Animals and the procedures approved by the IACUC (2017–0287-IBT and 2020–0232-IBT). Male Sprague–Dawley (SD) rats (3-week-old) were purchased from ENVIGO (Indianapolis, IN), housed in a room with a barrier system, and maintained at 23 ± 2°C, 55 ± 5% relative humidity, and a 12h light–dark cycle, with free access to chow and drinking water. After 3 weeks of acclimatization, rats were fed with 4NQO water for OPL induction. 4NQO (N0250, TCI America) was dissolved in propylene glycol to make a 4mg/mL stock solution and diluted to 50μg/mL (50 ppm) in acidified distilled water [39–42]. Throughout the feeding process (10–16 weeks), rats were monitored for their body weight, food/water intake, and motor activity. 4NQO water was replaced twice

a week. After 8–10 weeks of 4NQO feeding, incisional biopsies were taken from mucosal lesions on the dorsal tongue surface for histopathological diagnosis every other week (Figure S6A). Rats with histologically confirmed OEDs were withdrawn from 4NQO feeding and received patch treatment. The remaining lesions were treated for 2h a day for 5 consecutive days. Punch biopsies were taken to determine the efficacy of patch treatment 10 days after the last dose of patch treatment. Lesions were graded as 0, 1, 2, or 3 for no dysplasia, low-grade dysplasia (≤½ epithelial thickness), high-grade dysplasia (>½ epithelial thickness), or invasive carcinoma, respectively.

5.2 Combination index (CI) and isoborogram

Dysplastic oral keratinocyte (DOK) cells were purchased from Sigma-Aldrich (Cat# 94122104) with Certificate of DNA Profile Analysis and grown in DMEM supplemented with 10% FBS, 2mM glutamine, and 5μg/ml hydrocortisone. Tumor growth-inhibitory curves based on the MTT assay were plotted over a range of five drug concentrations with three-fold increment. The half-inhibitory concentrations (IC_{50}) were calculated using the Calcusyn program (Biosoft, Ferguson, MO). Drug interaction effects were measured by mixing two drugs at a 4-to-1, 2-to-1, 1-to-1, 1-to-2, or 1-to-4 ratio of their respective IC_{50} concentrations. Each combination was tested for its tumor growth-inhibitory effect over a range of five different dosages. CI values were calculated from 3–4 independent experiments using the Calcusyn program.

5.3 Patch formulation

Patch was designed to contain multiple layers of bioadhesive materials and drugs on a supportive frame (Tegaderm™ transparent film). The supportive frame prevents water leakage without affecting oxygen permeation. Fabrication was carried out using a CELLINK_BIO_X_3D printer. Bioadhesive materials include polyacrylic acid (PAA, Carbopol® 974 polymer), gelatin-modified dopamine (DOPA), and carboxymethyl cellulose (CMC). To fabricate a single-layered OXP-MPS patch, bioadhesive materials, including 0.1gm of polyacrylic acid-974 (PAA-974), 0.1gm of DOPA, and 0.2gm of CMC, were mixed with 1.5mg of OXP (102544–196, Sigma) and 20mg of MPS (1448989, Sigma), dissolved in 10ml distilled water, and blended in a Thinky Mixer (ARE-310, THINKY USA Inc.) for 40 minutes to form a homogenous aqueous solution. The mixed solution was added to a syringe with a 300μm diameter nozzle and printed in a square sheet (30mm × 30mm×20μm, containing 48.56μg of OXP and 648μg of MPS) directly on the supportive frame. During the printing process, the flow rate was controlled by adjusting the dispensing pressure, the valve opening time, and the dosing distance. The width of the printed lines was controlled by adjusting the printing speed and the parameters mentioned above. To fabricate a double-layered OXP-MPS v6.4 patch (30mm×30mm×20μm) with a top-to-bottom drug ratio of 1-to-2 (Figure 1C1), bioadhesive materials were prepared as described above, evenly divided into two parts, and mixed with OXP and MPS in the amounts of 0.5mg/6.67mg (OXP/MPS) for the top layer and 1.0mg/13.33mg for the bottom layer. Square sheets (30mm×30mm) were printed directly onto the supportive frame layer by layer (Figure 1B), with a 24-hour drying time at 37°C after each layer was printed, reducing the thickness down to 20μm. For testing and application, circular patches of different diameters were punched using a Miltex biopsy punch with plunger (4MD Medical, Lakewood, New Jersey).

5.4 UPLC-PDA (Ultra-Performance Liquid Chromatography with Photo-Diode-Array detector)

UPLC-PDA was used to measure the amounts of OXP and MPS in the patch. 5mm-diameter circular discs of patch samples were sonicated in 1mL H_2O for 20 minutes in an ice-water bath and vortexed. 45μL of supernatant was mixed with 5μL of 10× working buffer, 10μL of internal standard (AMP 50μg/mL, WF 100μg/mL), and 200μL of acetonitrile/0.01% ammonium hydroxide. 10μL of the mixture was injected into UPLC and detected by PDA. Assays were linear from 0.1μg/mL to 10.0μg/mL for OXP and from 0.1μg/mL to 50.0μg/mL for MPS. The accuracy and precision were within acceptable criteria of 10% for both assays.

5.5 LC-MS/MS

The amounts of OXP and MPS in the plasma were measured by the LC-MS/MS methods developed in our laboratory [43, 44]. The amounts of OXP and MPS in the plasma were measured using LC-MS/MS with a Shimadzu Nexera X2 UPLC (Columbia, MD) and a 4000 QRRAP® MS/MS system (AB Sciex, Redwood City, CA). System control and data analysis were performed using Analyst® software 1.6.2 (Sciex, Redwood City, CA). To measure the amount of OXP in the plasma, 20μL of sample was mixed with 4μL of internal standard (antipyrine 100 ng/mL) and 80μL of acetonitrile/0.01% ammonium hydroxide, and 10μL of the mixture was injected into LC-MS/MS. Chromatographic separation of MPS was performed on an ACE Excel 2 Super C_{18} column (50×2.1mm, 2μm, UK) with a binary solvent system of 0.1% formic acid in water (solvent A) and 0.1% formic acid in acetonitrile (solvent B). Chromatographic separation of OXP was performed on a Phenomenex Lux 5u Cellulose-1 column (250×4.6mm, 5μm) with an isocratic elution of 50% acetonitrile in water containing 1.25mM ammonia formate. The injection volume was 5μL, the total run time was 5.5 minutes, and the flow rate was 0.8mL/min. Tandem mass spectrometry was employed under positive ESI to detect the specific precursor to product ion transitions m/z 398.1 306.0 for oxaliplatin and m/z 189.0 131.0 for IS. Source parameters including ion spray voltage, temperature, nebulizer gas and heater gas pressure were set at 5000V, 700°C, 60 and 55 psi, respectively. The linear response ranged from 10ng/mL to 2500ng/mL ($r^2 > 0.990$). The LLOQ for OXP and MPS by our LC-MS/MS methods is 10ng/mL and 0.5ng/mL, respectively.

5.6 In vitro drug release test

In vitro drug release profiles were tested in aqueous solution, where individual OXP-MPS patches in 5mm-diameter circular discs were immersed in 1.5mL distilled water in a Slide-A-Lyzer™ MINI dialysis device at 37°C. At designated time points (10, 30, 60, 120, 180, and 240 minutes), 1 mL of the solution was collected from the device and replenished with the same amount of fresh distilled water. Collected solution was filtered through 0.45μm nylon filters and quantified for the amounts of OXP and MPS by UPLC-PDA. Six samples were repeated for each timepoint. The amounts of cumulative release were reported as mean ± standard deviation.

5.7 Side leakage test

Drug leakage from the side of the v6.4 patch was measured in the Franz Diffusion Cell Apparatus. A 9mm-diameter circular disc of patch was adhered to the undersurface of the porous membrane and immersed in the bottom receptor chamber, containing 5 mL of water and maintained at 37°C. The donor chamber was filled with water. Aliquots of solution (1 mL) from the receptor chamber were sampled for drug measurement at different timepoints (10 minutes, 30 minutes, 1 hour, 2 hours, and 4 hours), and calculated as percentages of the extractable drug amounts from the patch.

5.8 Ex vivo mucosal permeation test

Porcine buccal tissue was purchased from a local slaughterhouse (J&J Packing Company, Inc). The buccal mucosa was prepared by trimming the buccal tissue down to a 5–7mm thickness and mounted between the donor and receptor chambers of a Franz Diffusion Cell Apparatus. A v6.4 patch (d = 9mm) was then attached to the mounted buccal mucosa, with its bioadhensive layer facing down in the donor chamber. Both the donor and receptor chambers were filled with water and maintained at 37 °C. The receptor chamber solution was stirred at 400 rpm. The amounts of OXP and MPS permeating through the the buccal mucosa into the receptor chamber were measured by LC-MS/MS at 10 minutes, 30 minutes, 1 hour, 2 hours, and 4 hours. The amounts of drugs remaining in the buccal mucosa and the patch after 4 hours were measured by LC-MS/MS and UPLC-PDA, respectively.

5.9 Mechanical property and bioadhesive strength tests

The mechanical strength of the v6.4 patch was measured by a texture analyzer (SMT1–22, TestResources Inc.). Tested samples had a width of 20mm, a gauge length of 6cm and a thickness of 0.4mm. The length between the clamps was set to 20mm and the speed of testing was set to 5 mm/min. From machine-recorded data, the stress-strain relationship was calculated based on the following equations: (1) stress (σ) = F/A, where F is the applied force and A is the cross-sectional area, and (2) strain (ε)= ΔL/L, where ΔL is the change in length and L is the length between the clamps. Elastic modulus was calculated by the slope of the linear regression line best fitting for the initial linear part of the stress-strain curve. Adhesion force was measured using the same texture analyzer. A piece of porcine mucosa was fixed to the base of the test machine, and a patch was attached to the upper probe of the test machine through a clamp. Adhesion was done by adding 10μL water to the mucosal surface and immediately lowering the probe to allow contact between the patch and the mucosa. After applying a 5N force for 30s, the probe was lifted upwards at a speed of 5 mm/min. Adhesion force (in newton, N) was recorded as the force required to detach the patch from the mucosal surface.

5.10 Ex vivo mucoadhesion test

Mucosal tissues were harvested from pig buccal membrane and fixed on glass slides with glue. Patches were wetted in simulated saliva for 10 seconds, mounted on the porcine mucosa with light pressure, held for 30 seconds, and submerged in simulated saliva at 37°C. A total of 12 patches were mounted. The number of patches remaining on the mucosa surface were counted at the indicated time points (0h, 1h, 1.5h, 2h, 2.5h, 3.5h, and 4h).

5.11 In vivo mucoadhesion and drug release tests

SD rats (6–8 weeks old) were anesthetized by isoflurane using an induction chamber first and then a custom-made 8-way distributor manifold connected to nasal masks with individual ball valves for separate control over the isoflurane flow rate for maintenance. Circular discs of 3mm or 4mm diameter were punched from the mucoadhesive patch using a Miltex biopsy punch, moisturized with 1–2μl sterile water, and placed on the dorsal tongue or buccal mucosa with light pressure. For *in vivo* mucoadhesion tests, rats were given patches of 3mm or 4mm diameter on different locations and examined at different time points (0.5, 1, 1.5, 2, 3, or 4 hours) to determine whether the patch detached. Eight to ten rats were independently tested for every patch size, location, and timepoint. For *in vivo* drug release tests, SD rats received a 4-mm patch on the dorsal tongue surface and sacrificed at fixed timepoints (0.5, 1, 2, 3, or 4 hours) to collect tongue tissue samples underneath or surrounding the patch and plasma samples for LC-MS/MS analyses. For two additional sets of rats, patches were applied on the dorsal tongue surface for 4 hours and removed. Tongue tissues and plasma samples were collected at 4 and 8 hours after patch removal.

5.12 Histopathological analysis

Tongue lesions were collected by incisional or punch biopsy, fixed in 10% buffered formalin, embedded in paraffin blocks, and sectioned for H&E staining. Sections were coded in a double-blind manner and examined by a board-certified oral pathologist. Hyperplasia is defined as thickening (increased cell number) of the spinous cell layer of the surface epithelium without cellular atypia. Dysplasia is defined by the presence of atypical cellular and/or architectural changes, indicating abnormal maturation. Those changes include hyperchromatism, pleomorphism, increased nuclear-to-cytoplasmic ratio, rounding of the rete ridges, nuclear crowding, multi-nucleation, and dyskeratosis. Low-grade and high-grade dysplasia are defined by cellular and/or architectural atypia present within or beyond the lower half of the epithelium, respectively. Oral squamous cell carcinoma is defined as a malignancy arising from the surface squamous epithelium that has broken through the basement membrane and invaded the underlying tissue, such as the skeletal muscle.

5.13 Statistical analysis

Statistical analyses were performed using Microsoft Excel (Microsoft Office 2007 Ultimate edition) and GraphPad Prism software package (Version 5; GraphPad software, Inc., La Jolla, CA, USA). All data were analyzed without pre-processing. Continuous data (all except the efficacy study) were presented as mean ± s.e.m. and statistical differences between groups were analyzed by the two-tailed student t-test. Categorical data (*e.g.*, the efficacy study) were analyzed by the Chi-square test. P values below 0.05 were considered statistically significant. Error-bars represent mean ± s.e.m, as indicated in the figure legends.

Supplementary Material

Refer to Web version on PubMed Central for supplementary material.

Acknowledgements

This work is supported by Cancer Prevention and Research Institute of Texas (CPRIT) Early Translational Research Award (ETRA) RP170179 to Robert Y Tsai and Xiaohua Liu, CPRIT Core Facility Support Award (CFSA) RP180748 to Dong Liang and Huan Xie, National Institute of Dental and Craniofacial Research (NIDCR) DE024343 to Xiaohua Liu, and Texas A&M T3 Triads for Transformation Award to Robert Y Tsai and Yi-Shing Cheng.

References

1. Neville BW, et al., Squamous cell carcinoma. In Oral and Maxillofacial Pathology (St. Louis: Saunders Elsevier). 2016: p. 409–21.
2. Jemal A, et al. , Cancer statistics, 2009. CA Cancer J Clin, 2009. 59(4): p. 225–49. [PubMed: 19474385]
3. Chi AC, Leukoplakia (Leukokeratosis; erythroleukoplakia), in Oral and Maxillofacial Pathology, Neville BW, et al., Editors. 2016, Saunders Elsevier: St. Louis. p. 355–363.
4. Lippman SM, et al. , Comparison of low-dose isotretinoin with beta carotene to prevent oral carcinogenesis. N Engl J Med, 1993. 328(1): p. 15–20. [PubMed: 8416267]
5. Chiesa F, et al. , Follow-up of oral leukoplakia after carbon dioxide laser surgery. Arch Otolaryngol Head Neck Surg, 1990. 116(2): p. 177–80. [PubMed: 2297409]
6. Chiesa F, et al. , Risk of preneoplastic and neoplastic events in operated oral leukoplakias. Eur J Cancer B Oral Oncol, 1993. 29B(1): p. 23–8. [PubMed: 8180572]
7. Benner SE, Lippman SM, and Hong WK, Current status of chemoprevention of head and neck cancer. Oncology (Williston Park), 1992. 6(8): p. 61–6; discussion 66–8, 71 passim.
8. van der Hem PS, et al. , The results of CO2 laser surgery in patients with oral leukoplakia: a 25 year follow up. Oral Oncol, 2005. 41(1): p. 31–7. [PubMed: 15598583]
9. Roodenburg JL, Panders AK, and Vermey A, Carbon dioxide laser surgery of oral leukoplakia. Oral Surg Oral Med Oral Pathol, 1991. 71(6): p. 670–4. [PubMed: 1905797]
10. Vedtofte P, et al. , Surgical treatment of premalignant lesions of the oral mucosa. Int J Oral Maxillofac Surg, 1987. 16(6): p. 656–64. [PubMed: 3125262]
11. Holmes J. and Dierks E, Oral cancer treatment, in Peterson's Principles of Oral and Maxillofacial Surgery, Miloro M, et al., Editors. 2012, People's Medical Publishing House-USA: Shelton. p. 693–725.
12. Kofuji S, et al. , IMP dehydrogenase-2 drives aberrant nucleolar activity and promotes tumorigenesis in glioblastoma. Nat Cell Biol, 2019. 21(8): p. 1003–1014. [PubMed: 31371825]
13. Allison A. and Eugui E, Mycophenolate mofetil and its mechanisms of action. Immunopharmacology, 2000. 47(2–3): p. 85–118. [PubMed: 10878285]
14. Sweeney M, Mycophenolic acid and its mechanism of action in cancer and psoriasis. Japan J Antibiot, 1977. 30(Suppl): p. 85092.
15. Behrend M, Adverse gastrointestinal effects of mycophenolate mofetil: aetiology, incidence and management. Drug Saf, 2001. 24(9): p. 645–63. [PubMed: 11522119]
16. Lin T, Meng L, and Tsai RY, GTP depletion synergizes the anti-proliferative activity of chemotherapeutic agents in a cell type-dependent manner. Biochem Biophys Res Commun, 2011. 414(2): p. 403–8. [PubMed: 21971546]
17. Buell JF, Gross TG, and Woodle ES, Malignancy after transplantation. Transplantation, 2005. 80(2 Suppl): p. S254–64. [PubMed: 16251858]
18. Birkeland SA and Hamilton-Dutoit S, Is posttransplant lymphoproliferative disorder (PTLD) caused by any specific immunosuppressive drug or by the transplantation per se? Transplantation, 2003. 76(6): p. 984–8. [PubMed: 14508366]
19. Patel VF, Liu F, and Brown MB, Advances in oral transmucosal drug delivery. J Control Release, 2011. 153(2): p. 106–16. [PubMed: 21300115]
20. Roy SK and Prabhakar B, Bioadhesive Polymeric Platforms for Transmucosal Drug Delivery Systems - a Review. Tropical Journal of Pharmaceutical Research, 2010. 9(1): p. 91–104.

21. Sudhakar Y, Kuotsu K, and Bandyopadhyay AK, Buccal bioadhesive drug delivery - A promising option for orally less efficient drugs. Journal of Controlled Release, 2006. 114(1): p. 15–40. [PubMed: 16828915]
22. Hua S, Advances in Nanoparticulate Drug Delivery Approaches for Sublingual and Buccal Administration. Front Pharmacol, 2019. 10: p. 1328. [PubMed: 31827435]
23. Tang XH, et al. , Oral cavity and esophageal carcinogenesis modeled in carcinogen-treated mice. Clin Cancer Res, 2004. 10(1 Pt 1): p. 301–13. [PubMed: 14734483]
24. Kanojia D. and Vaidya MM, 4-nitroquinoline-1-oxide induced experimental oral carcinogenesis. Oral Oncol, 2006. 42(7): p. 655–67. [PubMed: 16448841]
25. Crawford M, et al. , Nucleostemin upregulation and STAT3 activation as early events in oral epithelial dysplasia progression to squamous cell carcinoma. Neoplasia, 2021. 23(12): p. 1289–1299. [PubMed: 34785448]
26. Lin T, et al. , Tumor-initiating function of nucleostemin-enriched mammary tumor cells. Cancer Res, 2010. 70(22): p. 9444–52. [PubMed: 21045149]
27. Graham MA, et al. , Clinical pharmacokinetics of oxaliplatin: a critical review. Clin Cancer Res, 2000. 6(4): p. 1205–18. [PubMed: 10778943]
28. Reardon JT, et al. , Efficient nucleotide excision repair of cisplatin, oxaliplatin, and Bis-aceto-ammine-dichloro-cyclohexylamine-platinum(IV) (JM216) platinum intrastrand DNA diadducts. Cancer Res, 1999. 59(16): p. 3968–71. [PubMed: 10463593]
29. Starobova H. and Vetter I, Pathophysiology of Chemotherapy-Induced Peripheral Neuropathy. Front Mol Neurosci, 2017. 10: p. 174. [PubMed: 28620280]
30. Crawford M, et al. , On the Cutting Edge of Oral Cancer Prevention: Finding Risk-Predictive Markers in Precancerous Lesions by Longitudinal Studies. Cells, 2022. 11(6).
31. Desai KGH, Polymeric drug delivery systems for intraoral site-specific chemoprevention of oral cancer. J Biomed Mater Res B Appl Biomater, 2018. 106(3): p. 1383–1413. [PubMed: 28650116]
32. Nishimura A, Changes in Bcl-2 and Bax expression in rat tongue during 4-nitroquinoline 1-oxide-induced carcinogenesis. J Dent Res, 1999. 78(6): p. 1264–9. [PubMed: 10371251]
33. Sato K, et al. , Expression of beta-catenin in rat oral epithelial dysplasia induced by 4-nitroquinoline 1-oxide. Oral Oncol, 2002. 38(8): p. 772–8. [PubMed: 12570056]
34. Nauta JM, et al. , Comparison of epithelial dysplasia--the 4NQO rat palate model and human oral mucosa. Int J Oral Maxillofac Surg, 1995. 24(1 Pt 1): p. 53–8. [PubMed: 7782642]
35. Hecht SS, Cigarette smoking and lung cancer: chemical mechanisms and approaches to prevention. Lancet Oncol, 2002. 3(8): p. 461–9. [PubMed: 12147432]
36. Luo FR, Wyrick SD, and Chaney SG, Biotransformations of oxaliplatin in rat blood in vitro. J Biochem Mol Toxicol, 1999. 13(3–4): p. 159–69. [PubMed: 10098901]
37. Luo FR, et al. , High-performance liquid chromatographic separation of the biotransformation products of oxaliplatin. J Chromatogr B Biomed Sci Appl, 1999. 724(2): p. 345–56. [PubMed: 10219677]
38. Jerremalm E, Wallin I, and Ehrsson H, New insights into the biotransformation and pharmacokinetics of oxaliplatin. J Pharm Sci, 2009. 98(11): p. 3879–85. [PubMed: 19340883]
39. Sakaki T, et al. , Changing expression of E- and P-cadherin during rat tongue carcinogenesis induced by 4-nitroquinoline 1-oxide. J Oral Pathol Med, 2003. 32(9): p. 530–7. [PubMed: 12969227]
40. Moon SM, et al. , Homeobox C5 expression is associated with the progression of 4-nitroquinoline 1-oxide-induced rat tongue carcinogenesis. J Oral Pathol Med, 2012. 41(6): p. 470–6. [PubMed: 22385119]
41. Kong X, et al. , Analysis of plasma metabolic biomarkers in the development of 4-nitroquinoline-1-oxide-induced oral carcinogenesis in rats. Oncol Lett, 2015. 9(1): p. 283–289. [PubMed: 25435976]
42. Ohnishi Y, et al. , Usefulness of a fluorescence visualization system for the detection of oral precancerous and early cancerous lesions. Oncol Rep, 2016. 36(1): p. 514–20. [PubMed: 27121913]

43. Gao X, et al. , Determination of Oxaliplatin by a UHPLC-MS/MS Method: Application to Pharmacokinetics and Tongue Tissue Distribution Studies in Rats. Pharmaceuticals (Basel), 2021. 15(1).

44. Gao X, et al. , Determination and validation of mycophenolic acid by a UPLC-MS/MS method: Applications to pharmacokinetics and tongue tissue distribution studies in rats. J Chromatogr B Analyt Technol Biomed Life Sci, 2020. 1136: p. 121930.

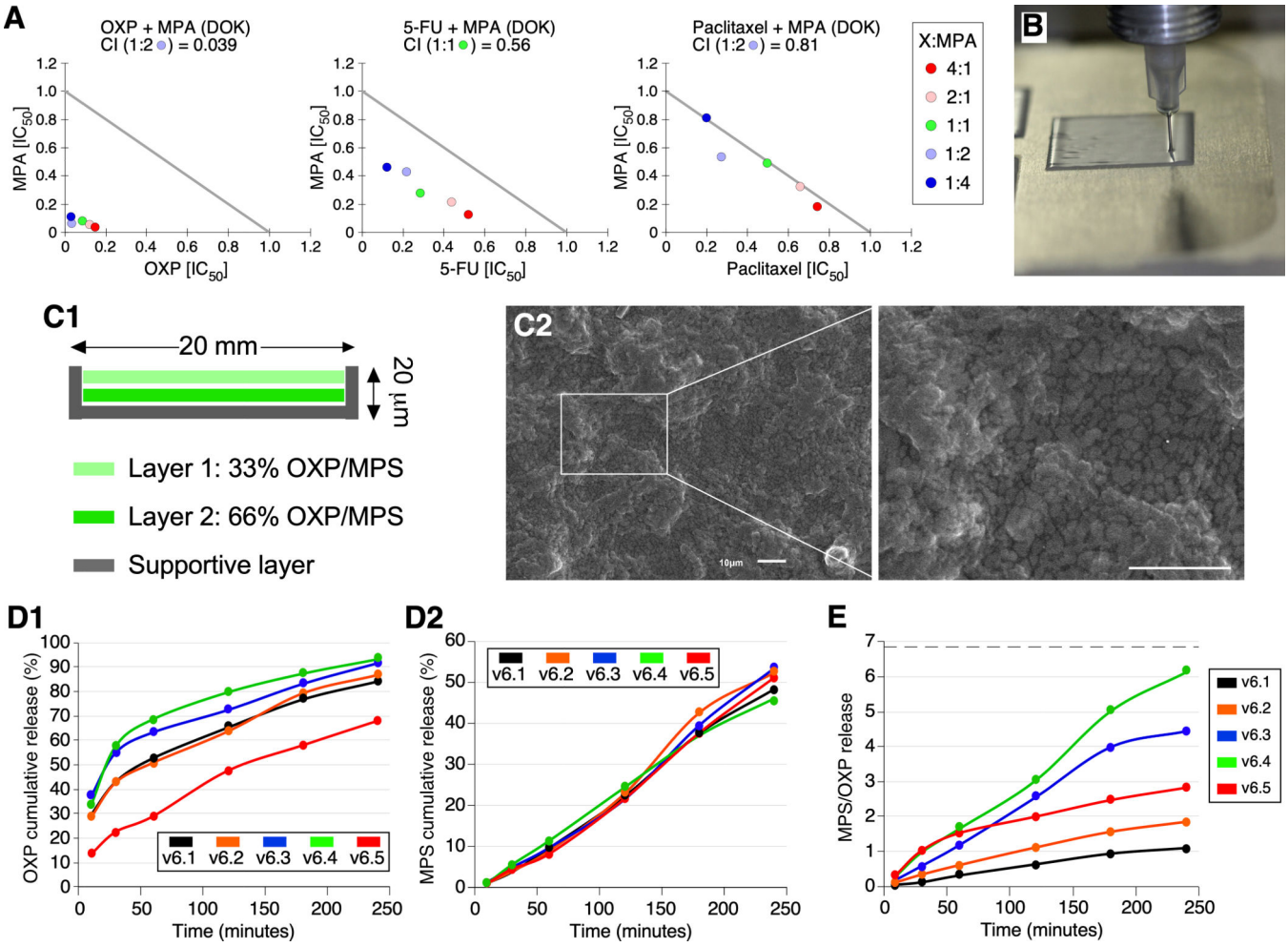

Figure 1. Formulations and *in vitro* drug release profiles of the OMP-MPS v6 patches.

(**A**) Drug interaction between MPA and OXP, 5-FU, or paclitaxel was determined by their respective combination indices (CIs). Five different drug-to-MPA ratios with different color labels were examined, with the 1-to-1 ratio representing each drug at equivalent amounts of their respective IC_{50} concentrations. Numbers on top list the smallest CIs for each combination. (**B**) A mucoadhesive patch underwent 3-D printing. (**C1**) Schematic diagram of a cross-sectional view showing the supportive frame (grey) and two layers of drug-embedded bioadhesive materials (green). (**C2**) SEM image of the OXP-MPS ChemoPatch. Right panel shows an enlarged area of the left panel, indicated by the white box. Scale bars show 10µm. (**D**) Five variations of the 6th generation (v6) patches were designed to contain two bioadhesive drug layers with the same total amount of MPS and different amounts of OXP (see text). The cumulative release profiles of OXP (**D1**) and MPS (**D2**) into water solution from 0 to 4 hours (4h) was presented percentages of their respective total extractable amounts. (**E**) Ratios between the cumulative released amounts of MPS and OXP (in weight) by the v6 patches over a 4h period. An MPS/OXP weight ratio of 6.9 (dashed line) equals an IC_{50} ratio of 1.

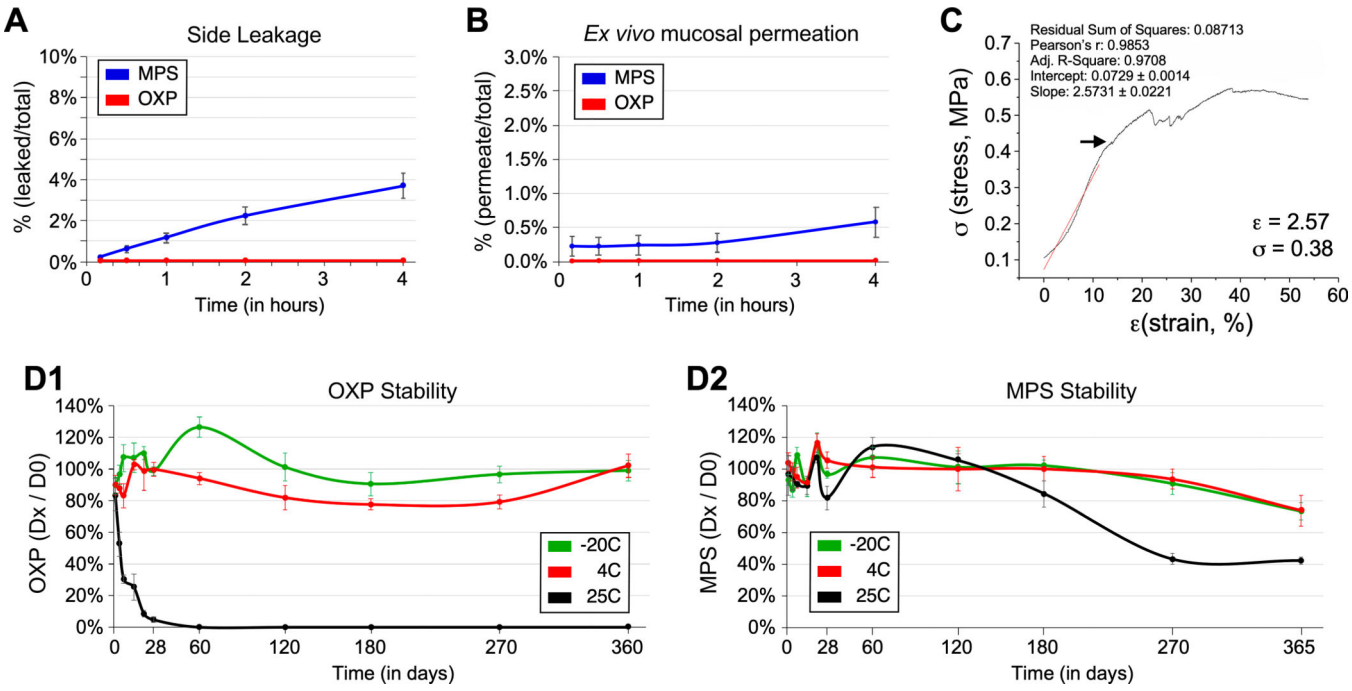

Figure 2. Side leakage, mucosal permeation, mechanical strength, and drug stability of the OXP-MPS v6.4 patch.

(**A**) Cumulative leakage of OXP (red) MPS (blue) from the side of a 9mm-diameter disc of the v6.4 patch was measured at 10 minutes (10m), 30m, 1h, 2h, and 4h, and expressed as percentages of their respective total extractable amounts in the patch. (**B**) The amounts of OXP (red) and MPS (blue) passing through a porcine mucosal layer from an attached v6.4 patch (9mm-diameter disc) were measured at 10m, 30m, 1h, 2h, and 4h and expressed as percentages of their respective total extractable amounts in the patch. (**C**) The mechanical strength of the v6.4 patch was determined by its stress (σ, in MPa)-strain (ε) curve measured using a TestResources System. Red line represents the best-fitting linear regression line of the initial slope of the stress-strain curve. Arrow indicates membrane breakpoint. (**D**) The amounts of OXP (**D1**) and MPS (**D2**) remaining in the OXP-MPS patch kept at 25°C (*black*), 4°C (*red*), or −20°C (*green*) for 1 day (1d), 4d, 7d, 14d, 21d, 28d, 60d, 120d, 180d, 270d, and 360d were quantified and expressed as percentages of their respective amounts extracted from freshly made patches (n=5). OXP and MPS were measured by LC-MS/MS in (**A**, **B**) or UPLC-PDA in (**D**).

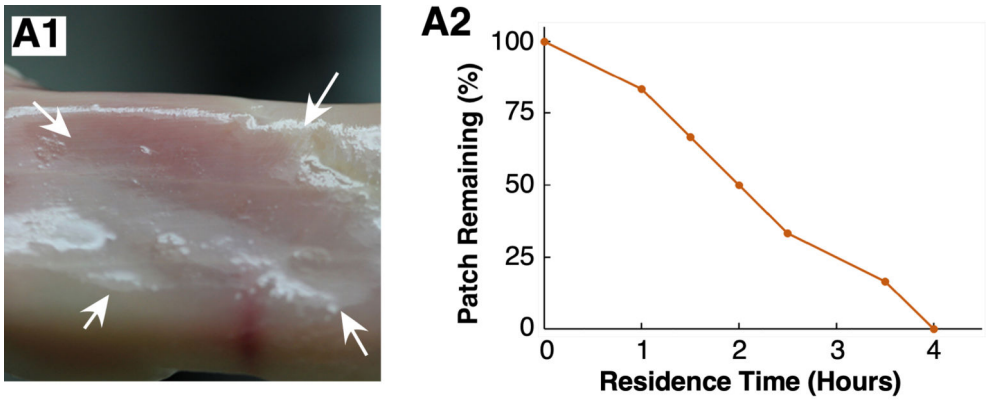

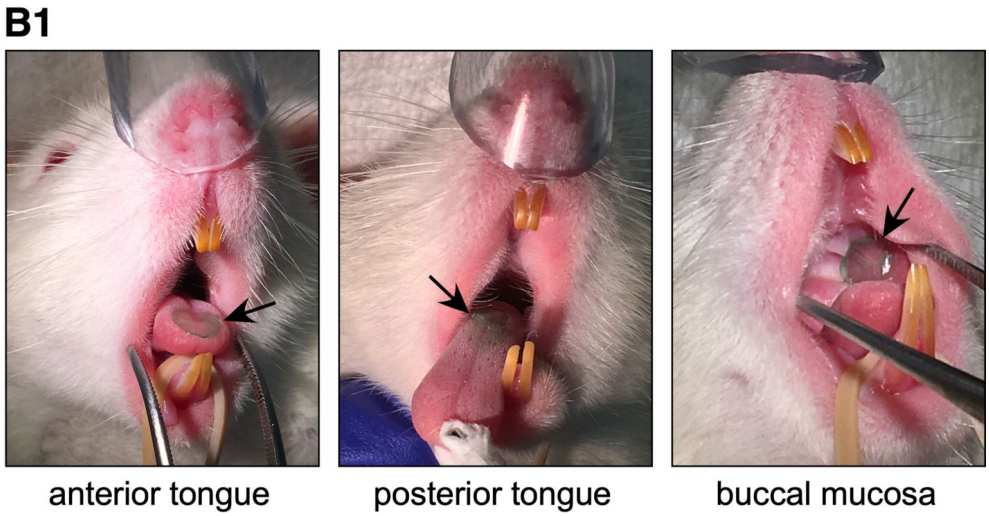

B2

Diameter	Site	Timepoint					
		0.5 h	1 h	1.5 h	2 h	3 h	4 h
4 mm	Ant-Tg	8/8	8/8	8/8	8/8	8/8	8/8
	Post-Tg	8/8	8/8	8/8	7/8	8/8	8/8
	Buccal	10/10	10/10	9/10	10/10	10/10	10/10
3 mm	Ant-Tg						8/8
	Post-Tg			n.d.			8/8
	Buccal						10/10

Figure 3. *In vitro* and *in vivo* mucoadhesive tests.

(**A1**) *Ex vivo* residence time of the OXP-MPS v6.4 patch (corners indicated by arrows) on top of a porcine oral mucosa. (**A2**) The percentage of patches adhering to the mucosal surface after immersion in simulated saliva for 1-to-4h (n = 12). (**B1**) *In vivo* residence time of the v6.4 patch (green, indicated by arrows) on the anterior tongue, posterior tongue, or buccal mucosa of SD rats under anesthesia. (**B2**) The number of patches adhering to the mucosa over the number of patches tested at 0.5-to-4h after placement. Tg, tongue; n.d., not determined.

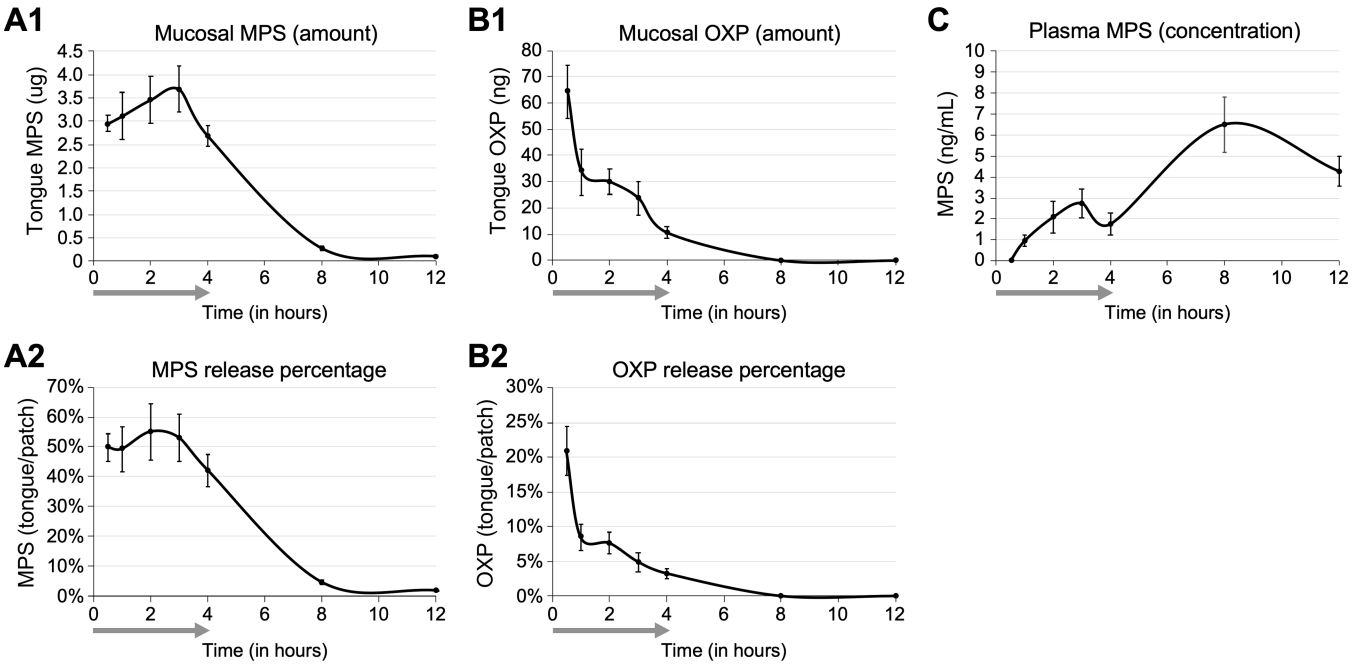

Figure 4. ***In vivo*** **drug release profiles of the OXP-MPS v6.4 patch.**

Rats were given 4mm-diameter circular discs of the OXP-MPS v6.4 patch on their dorsal tongue surface and sacrificed after 0.5h, 1h, 2h, 3h, or 4h (8 per group). Two additional groups were given a 4h patch application and sacrificed at 4h and 8h after the removal of the patch. Samples were collected from tongues tissue (**A**, **B**) and plasma (**C**) for drug measurement by LC-MS/MS (n = 8). Grey arrows indicate the patch treatment time.

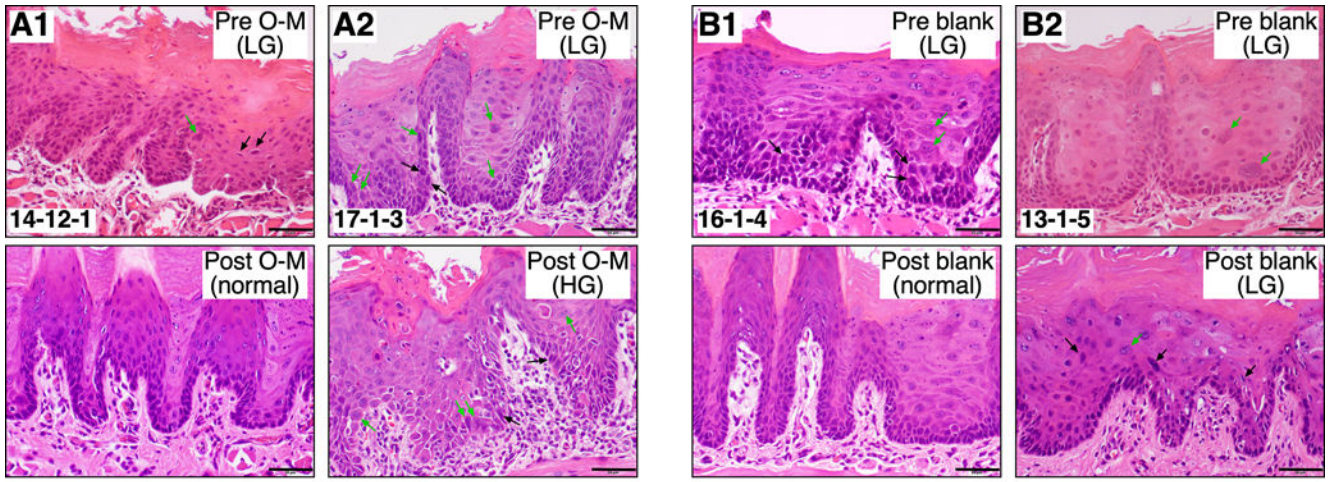

C

Patch	Treatment	Pre-patch biopsy		Post-patch biopsy (10d)		No.
		Histopathology	Depth	Histopathology [Grade]	Depth	
O-M	2h × 5d	low-grade dysplasia	≤ ½	normal epithelium [G0]	0	0
	2h × 5d	low-grade dysplasia	≤ ½	normal maturation w/ hyperkeratosis [G0*]	0	1
	2h × 5d	low-grade dysplasia	≤ ½	normal maturation w/ basilar hyperplasia [G0#]	0	7
	2h × 5d	low-grade dysplasia	≤ ½	low-grade dysplasia [G1]	≤ ½	0
	2h × 5d	low-grade dysplasia	≤ ½	high-grade dysplasia [G2]	> ½	1
	2h × 5d	low-grade dysplasia	≤ ½	SCC [G3]		0
blank	2h × 5d	low-grade dysplasia	≤ ½	normal epithelium [G0]	0	0
	2h × 5d	low-grade dysplasia	≤ ½	normal maturation w/ hyperkeratosis [G0*]	0	0
	2h × 5d	low-grade dysplasia	≤ ½	normal maturation w/ basilar hyperplasia [G0#]	0	2
	2h × 5d	low-grade dysplasia	≤ ½	low-grade dysplasia [G1]	≤ ½	5
	2h × 5d	low-grade dysplasia	≤ ½	high-grade dysplasia [G2]	> ½	0
	2h × 5d	low-grade dysplasia	≤ ½	SCC [G3]		3

D

	outcome (grade)		
	G0	≥G1	total
O-M	8	1	9
blank	2	8	10
total	10	9	19

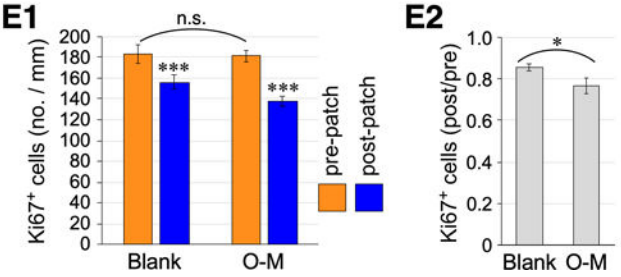

Figure 5. Efficacy of the OXP-MPS v6.4 patch in treating 4NQO-induced low-grade oral epithelial dysplasias (OEDs).

Low-grade OEDs on the dorsal surface of the tongue were confirmed by incisional biopsies and treated with the OXP-MPS patch (**A**) or the blank patch (**B**) for 2h×5d. Black arrows, dyskeratotic cells; green arrows, multi-nucleated cells. (**C**) Numbers of cases with different histopathological outcomes after 10d of recovery in the OXP-MPS (O-M) or blank patch treatment group. (**D**) Chi-square analyses of the efficacy of the O-M patch (n = 9) vs. the blank patch (n = 10) in reversing low-grade OEDs to normal epithelium ($p = 0.0027$). (**E**)

Effects of the O-M patch (n = 9) vs. the blank patch (n = 10) on the epithelial mitotic (Ki67) activity in the basal and parabasal layer analyzed by two-sided student t-test. Bar graphs show mean (± s.e.m); *, $p < 0.05$; n.s., not significance. Scale bars show 50μm in (**A**, **B**).

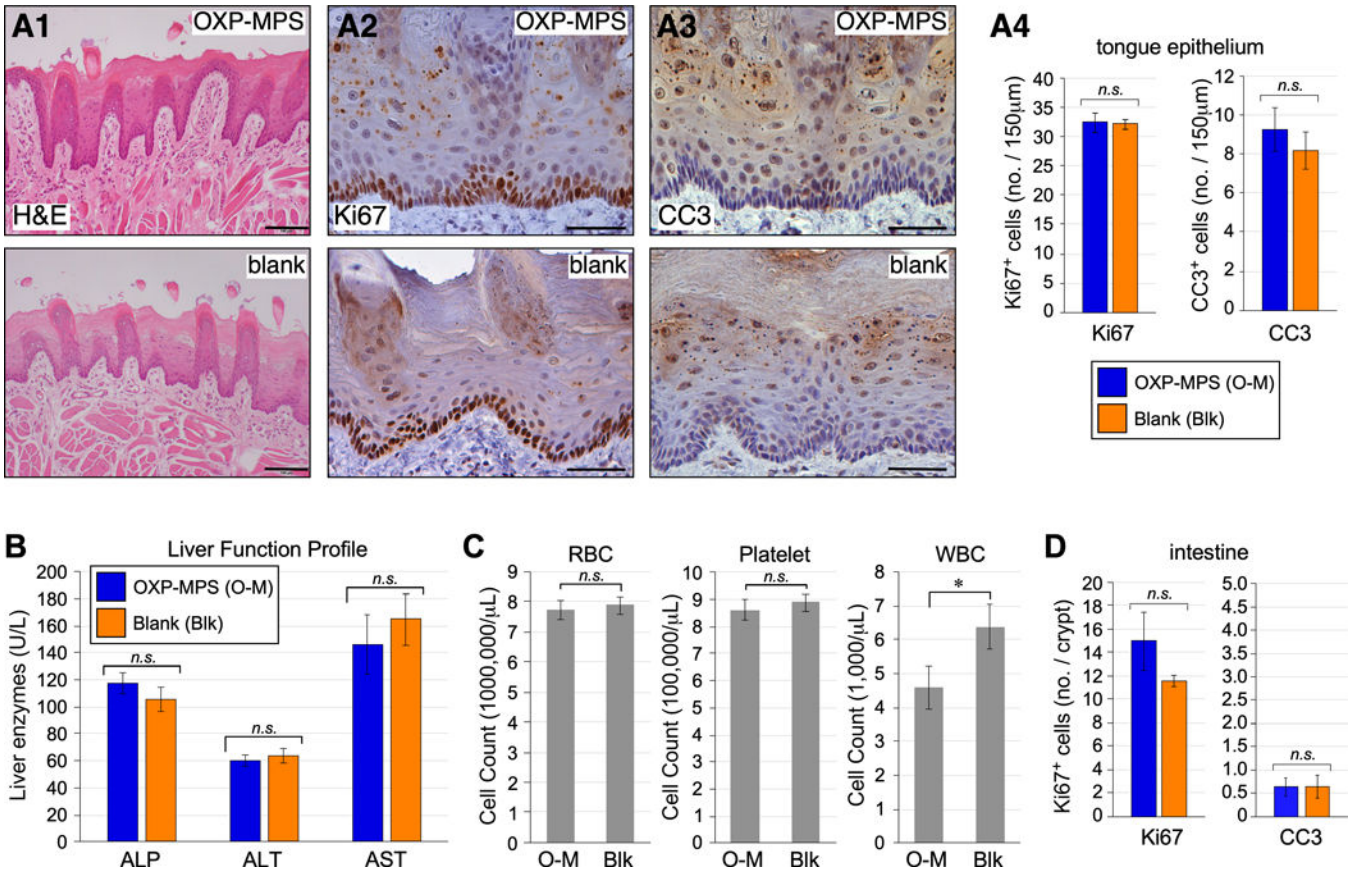

Figure 6. Local and systemic toxicities of the OXP-MPS v6.4 patch.

Toxicities were evaluated 48h after the completion of the patch treatment (4h×5d) in healthy SD rats. (**A**) Local toxicities were determined by H&E (**A1**), Ki67 (**A2**, and cleaved caspase 3 (CC3) (**A3**) staining of oral mucosa. (**A4**) Quantification of $Ki67^+$ and $CC3^+$ cells in tongue epithelium. Systemic toxicities were determined by liver function test (**B**) and complete blood count (**C**). (**D**) Quantification of $Ki67^+$ and $CC3^+$ cells in intestinal epithelium. Scale bars show 100μm in (**A1**) and 50μm in (**A2**, **A3**). ALP, alkaline phosphatase; ALT, alanine aminotransferase; AST, aspartate aminotransferase; WBC, white blood cells; RBC, red blood cells. Bar graphs show mean (± s.e.m). Differences between the O-M patch (n = 12) and the blank patch (n = 10) group were analyzed by two-sided student t-test and determined as significant with p values ≤ 0.05 (*) or not significant (n.s.) with p values > 0.5.